Hydraulic conductivity, microstructure and texture of compacted claystone/ bentonite mixtures saturated with different solutions

M. Middelhoff, Olivier Cuisinier, Stéphane Gaboreau, F. Masrouri, J. Talandier, N. Michau

Hydraulic conductivity, microstructure and texture of compacted claystone/ bentonite mixtures saturated with different solutions

M. Middelhoff [1, 2 †], O. Cuisinier [1*], S. Gaboreau [3], F. Masrouri [1], J. Talandier [2], N. Michau [2]

[1] Université de Lorraine – LEMTA, UMR 7563 CNRS,
(2 Rue du Doyen Marcel Roubault - BP 10162, 54000 Nancy CEDEX, France)

[2] Agence nationale pour la gestion des déchets radioactifs (Andra), France

[3] Bureau de recherches géologiques et minières (BRGM), France

Olivier.Cuisinier@univ-lorraine.fr

Abstract: The French reference concept for the disposal of intermediate- and high-level nuclear waste in the Callovo-Oxfordian sedimentary rock formation (COX-claystone) considers the employment of crushed COX-claystone and its mixture with MX80-bentonite as potential backfill materials installed in drifts and shafts upon termination of the operational phase of the future repository. The fraction of MX80-bentonite in the mixture is limited to 30% in wet weight. Over time, the backfill will be saturated with solutions that originate in the surrounding rock formation and percolate through the concrete lining left in place. The main characteristic of the leachate will be its high pH-value. In addition to the swelling pressure, the sealing properties of the backfill are determined by the hydraulic conductivity. This laboratory experimental study aimed to understand the hydraulic conductivity evolution of potential backfill materials under realistic conditions in terms of compaction conditions, solution chemistry, temperature and hydraulic gradient, and to relate results determined at the macroscale to results of microstructural and textural analysis. Also, the impact of the solution chemistry was evaluated by these means. In the case of mixture-samples, no stabilization of hydraulic conductivity was detected, despite the duration of the experiments being about one year. There was no detectable impact of the solution chemistry in the course of experiments attributable to low reaction kinetics under imposed conditions. Subsequent microstructural analysis indicated material swelling triggering rearrangements in the pore space and lowering the fraction of hydraulic conductive voids. Interestingly, neither the saturation nor the solution chemistry had an impact on the texture of materials.

Keywords: Callovo-Oxfordian claystone, MX80-bentonite, Hydraulic conductivity, Microstructure, Texture, Solution chemistry

† currently contracted by: Gesellschaft für Anlagen- und Reaktorsicherheit (GRS) gGmbH, Theodor-Heuss-Straße 4, 38122 Braunschweig, Germany

1 Introduction and background

The French reference concept considers the disposal of intermediate and high level nuclear waste in the Callovo-Oxfordian sedimentary rock formation located 500 m below ground level (ANDRA, 2005). Henceforth, the sedimentary rock formation is referred to as Callovo-Oxfordian (COX) claystone. The encapsulated nuclear waste will be emplaced in horizontal drifts, which will be sealed and backfilled once the operational phase of the repository is terminated. Unlike the seals, backfill is envisaged to be installed in situ by means of conventional compaction techniques. It will swell upon its saturation and inhibit the flow of fluid phases from the emplacement drifts to accessible biosphere over time. Its installation particularly aims to limit the propagation of the excavation damaged/ disturbed zone (EDZ/ EdZ) and to close the hydraulic conductive pore space (ANDRA, 2005). In addition to the swelling pressure evolving under the constant volume conditions, the hydraulic conductivity can be considered as one of the key parameters which govern the sealing properties of backfill.

Potential backfill materials are re-employed COX-claystone and its mixture with MX80-bentonite. COX-claystone is obtained during drift excavation and processed afterwards. Henceforth, crushed and sieved COX-claystone is referred to as COX_c. Its re-employment particularly aims to inhibit mineralogical and physico-chemical incompatibilities with the surrounding rock formation (ANDRA, 2005). A mixture composed of COX_c and MX80-bentonite is considered alternatively, since the increased smectite fraction might enhance the barrier functions of backfill. Like other smectite-containing materials, COX_c and its mixture might be affected by variations in the material characteristics (e.g. textural and microstructural characteristics, initial dry density, degree of saturation etc.), the environmental conditions (e.g. solution chemistry etc.) and stress history (e.g. preconsolidation pressure, overburden pressure etc.) with regard to their hydro-mechanical behavior (e.g. Alonso et al., 1987; Chen, 1988). It must be thus evaluated whether the sealing characteristics of backfill are stable to possible variations over time.

According to Burland (1990), the structure of smectite-containing materials comprises fabric as well as interparticle bonding. Even though fabric also provides information about the arrangement of particles, this study adopts texture as it describes the features of particles (e.g. shape, orientation towards each other) and pores (e.g. shape, volume) more precisely.

Numerous laboratory experimental studies addressed the impact of the saturating solution chemistry on the physico-chemical and textural characteristics (e.g. Ramírez et al., 2005; Herbert et al., 2008), the microstructure (e.g. Cuisinier et al., 2008; Fernández et al., 2014) and the hydro-mechanical behavior of smectite-containing materials (e.g. Villar, 2006; Karnland et al., 2007; Cuisinier et al., 2014; Zhang and Kröhn, 2019; Middelhoff et al., 2020). Considering the French reference concept, the impact of the pH is of major relevance, as described below.

Once the closure phase of the repository is terminated, the backfill might be saturated with solutions, which originate in the surrounding geological formation and percolate through the concrete lining left in place. The initial leachate is characterized by a pH above 13.5. This elevated pH is attributable to the release of potassium and sodium hydroxides from the concrete. After their leachate, the solution chemistry will be controlled by the dissolution of portlandite at a pH of 12.5 and later by the dissolution of cement phases at a pH ranging from 10.5 to 12.5. The phenomenon is referred to as hyperalkaline plume and might trigger different geochemical reactions while saturating the backfill (Huertas et al., 2000; Michau, 2005). Ion exchange at clay minerals can be expected once the alkaline solution percolates the backfill material. For instance, sodium ions can be replaced by calcium ions from the alkaline solution as their hydration potential is higher (Norrish, 1954). Simultaneously, the dissolution of clay minerals can be triggered as they remain relatively stable up to a pH of 9 and start dissolving once the pH exceeds 10. Secondary minerals, such as carbonates, clay minerals, cement phases, silicates, and zeolites, can precipitate or form afterwards. Their reaction kinetics and reaction mechanism are controlled by the pH of solutions, among other factors (Krauskopf, 1956). The analyses of

concrete lining/ claystone formation-interfaces sampled in situ indicated low reaction kinetics under real conditions (Gaboreau et al., 2011; Gaboreau et al., 2012). Thus, in order to determine a considerable impact of the solution chemistry on the backfill, the clay mineral/ pore water-system needs to remain thermodynamically unstable for a sufficiently long time.

To investigate the impact of the solution chemistry on the backfill materials in a reasonable period of time, most studies considered either simplified or extreme conditions, instead of realistic conditions. Simplified or extreme conditions comprise an increased liquid to solid ratio, an increased ionic strength of solutions, the employment of homoionic solutions and an increased temperature. In the case of hydraulic conductivity experiments, values can be presumably obtained faster by imposing higher hydraulic gradients. However, there is no information about the impact of the magnitude of the hydraulic gradient on the reaction kinetics.

The impact of saturating solution chemistry on the physico-chemical and textural characteristics of smectite-containing materials is mainly investigated by conducting batch experiments characterized by a high liquid to solid ratio (e.g. Herbert et al., 2004; Hofmann et al., 2004; Ramírez et al., 2005; Fernández et al., 2014; Elert et al., 2015). However, there are significantly different results, particularly regarding the cation exchange capacity and specific surface area. Differences are attributable to the differences in the composition, ionic strength, and pH of solutions and in imposed temperatures. In general, results lack transferability to compacted materials predominantly due to the high liquid to solid ratio.

Micro-, meso- and macropores characterize the structure of compacted smectite-containing materials in the unsaturated state and correspond to pores between clay particles, clay aggregates, and greater assemblies of clay aggregates and shielding grains, respectively. The existence of meso- and macropores is indicated by a bi-modal pore-size distribution (PSD) which is commonly determined by means of mercury intrusion porosimetry (MIP) experiments

(Alonso et al., 1987). In addition, N_2-gas sorption experiments are performed to provide further information, in particular on the existence of some smaller mesopores and micropores.

There are only a few studies addressing the impact of solution chemistry, in particular its pH, on the microstructure of compacted smectite-containing materials. For instance, the study of Cuisinier et al. (2008) comprised an aging process, in which compacted clayey soil samples were saturated with a portlandite-saturated solution (pH > 12) under elevated temperatures (> 50°C). The aging process lasted longer than 12 months. Subsequent MIP-experiments revealed that the macropores increased significantly, whereas the mesopores remained stable. The dissolution of smectite accounted for the increase in the amount of macropores, and might in turn provoke an increase in hydraulic conductivity (Romero, 2013). In general, the results are less transferable to compacted backfill materials, since the elevated temperatures accelerated the reaction kinetics and might have induced different reaction mechanisms.

There is a wealth of studies aiming to analyze the impact of saturating solution chemistry on the hydraulic conductivity behavior of compacted backfill materials under realistic conditions (e.g. Mata, 2003; Villar, 2006; Ye et al., 2014; Zhang and Kröhn, 2019; Zhang, 2021). Realistic conditions refer to the initial compaction conditions of samples, the saturating solution chemistry, and the ambient temperature. Their major conclusion was that the impact vanishes upon the ionic strength decreases or the dry density increases. Results were attributed to the modification of the pore size distribution and to the mobility of the water molecules within the macropores. However, interpretations were mainly based on diffuse double layer (DDL) theories and thus lack direct experimental evidence.

Only a few studies related changes in the hydraulic conductivity behavior of smectite-containing materials to the impact of the saturating solution chemistry, in particular of the pH-value, on the physico-chemical and textural characteristics and microstructure (e.g. Pusch et al., 2003; Cuevas, 2005; Karnland et al., 2007; Cuisinier et al., 2014). Indeed, parts of the studies

of Pusch et al. (2003) and Cuevas (2005) were conducted under realistic conditions (e.g. compaction state, solution chemistry, ambient temperature) and are thus of special interest. However, both studies lacked completeness as they disregarded the microstructure and attributed changes in the hydraulic conductivity to the impact of the solution chemistry on the physico-chemical and textural characteristics only. Results indicated that the solution chemistry affected neither the hydraulic conductivity of materials nor their cation exchange capacity and specific surface area. Those observations were attributed to the low reaction kinetics. Despite the conclusion, the sealing properties of potential backfill materials were assumed to be long-term stable to the saturating solution chemistry under realistic conditions.

The literature review revealed that compared to the one-dimensional volume change behavior (e.g. compressibility, swelling pressure) the fluid transfer behavior of COX_c-based materials was little investigated although it determines the sealing behavior of the backfill. Former experiment programs also disregarded relevant boundary conditions, in particular the pH-value of saturating solutions. This study thus aims to determine the hydraulic conductivity of COX_c and its mixture with MX80-bentonite by means of constant-head experiments, whose conditions were believed to induce repository-like conditions in terms of compaction state, temperature, hydraulic gradient and solution chemistry. Subsequent N_2-gas sorption and mercury intrusion porosimetry (MIP) experiments serve the purpose of linking differences in the hydraulic conductivity to changes in the texture and microstructure of materials. In particular, the saturation of materials with a hyperalkaline solution is expected to induce considerable changes. The analyse of the spatial distribution of textural and microstructural parameters allow to assess whether the hydraulic conductivity is still evolving in the short- and intermediate-term or reflects a long-term stable state. The experimental program involving the saturation of materials with a hyperalkaline solution and the approach of linking directly the evolution of hydraulic conductivity to textural and microstructural changes constitute the uniqueness of this study.

2 Materials

The materials investigated were COX_c and its mixture with MX80-bentonite (Wyoming, USA). The mixture was composed of 70% COX_c and 30% MX80-bentonite in wet weight. The limitation of MX80-bentonite to 30% was based on the reasons mentioned above (e.g. reductions of incompatibilities with the surrounding formation). COX-claystone was obtained during the excavation of drifts of Andra's URL in a depth of – 490 m (Bure, Meuse/ Haute-Marne region, France). Conil et al. (2018) highlighted that the mineralogical composition, water content and porosity of intact COX-claystone samples vary with their position in the rock formation. Correspondingly, COX_c was expected to consist of about 46% phyllosilicates (e.g. illite, ordered illite/ smectite mixed layer minerals), 24% tectosilicates (e.g. quartz, feldspars), 27% carbonates (e.g. calcite, dolomite), and minor fractions of associated minerals (e.g. pyrite). In accordance with the reference concept, the subsequent processing of material comprised the crushing and sieving to a maximum grain size of 2 mm. The material was then stored in airtight containers. The wealth of information about the volume change, transfer, and sorption behavior of MX80-bentonite accounted for its selection to be mixed with COX_c. MX80-bentonite was supplied by Laviosa-MPC SAS (Limay, France), who already processed the material to a maximum grain size of 2 mm before filling it in airtight containers. It is noteworthy that the supplier indeed sells its bentonite from Wyoming under the commercial name of Expangel SP7, but it is commonly identified under the name of MX80. Its mineralogical composition is dominated by phyllosilicates (e.g. smectites), whose fraction is about 80%. Other minerals are tectosilicates (e.g. quartz, feldspars) and carbonates (e.g. calcite) (e.g. Molinero-Guerra et al., 2020).

Information about the physical and physico-chemical characteristics of COX_c and its mixture with bentonite are given in Table 1. Physical characteristics of COX_c and its mixture with MX80-bentonite were taken from Middelhoff et al. (2020). The external specific surface area (SSA) and the cation exchange capacity (CEC) of COX_c and the mixture were determined by

179 means of the BET- and cobalt hexamine methods (Orsini and Remy, 1976), respectively. The
180 latter was also employed to determine the exchangeable cation species. Values of SSA and CEC
181 of COX_c were in good agreement with previous studies (Gaucher et al., 2004; Yven et al., 2007).
182 The dominant exchangeable cation species in COX_c were Ca^{2+}, Mg^{2+}, Na^+ and K^+, listed ac-
183 cording to their amount encountered. Corresponding amounts were 53%, 21%, 13% and 12%
184 of adsorbed cations, respectively. The replacement of COX_c by 30% MX80-bentonite led to a
185 significant increase in the fraction of Na^+-ions. The exchangeable cations were then dominated
186 by Na^+-ions, followed by Ca^{2+}-, Mg^{2+}- and K^+-ions with respect to their amount. Corresponding
187 amounts were 43%, 36%, 15% and 6% of adsorbed cations, respectively.

188 The grain size distribution curves of COX_c and the mixture are shown in Figure 1. The
189 size distribution of grains smaller than 0.8 mm was measured by means of laser diffractometry
190 (ISO, 2009), whereas dry sieving was conducted in order to obtain the size distribution of the
191 residual grains. As depicted, the distribution curves of both materials were comparable. The
192 compaction behavior of both materials was investigated by means of standard and modified
193 Proctor experiments. Materials were prepared at various water contents by adding correspond-
194 ing quantities of deaired/ demineralized water. They were left in airtight containers for more
195 than one week occasionally revolved to guarantee the homogeneous distribution of added water.
196 A detailed description of results of standard and modified Proctor experiments and their inter-
197 pretation are given in Middelhoff et al. (2020). Modified Proctor experiments revealed that the
198 maximum dry density and optimum water content were 1.95 Mg/m^3 and 13.2%, respectively,
199 in the case of COX_c, and 1.72 Mg/m^3 and 18.2%, respectively, in the case of the mixture.

200 The laboratory experimental program comprised the saturation of both materials with
201 three solutions differing in their composition and properties. Deaired/ demineralized water
202 served as a reference solution. Henceforth, water referred to deaired/ demineralized water, and
203 the subscripts SS and AS indicated the artificial site solution and the artificial alkaline solution,

respectively. The compositions of the site and alkaline solution corresponded to the rock formation water and to solutions believed to evolve from percolating through the concrete lining, respectively. Both solutions were prepared according to a protocol established and provided by Andra (Middelhoff et al., 2020). Their compositions and key properties are given in Table 2. The site and the alkaline solutions were comparable in terms of the order of magnitude of their ionic strength, however the alkaline solution was characterized by an elevated pH. The pH of AS corresponded to the solution chemistry controlled by the dissolution of portlandite.

3 Experiments

The hydraulic conductivity, microstructure and texture of COX_c and its mixture with MX80-bentonite were determined by means of constant head experiments, mercury intrusion porosimetry (MIP) experiments and N_2-gas sorption experiments, respectively. The sample preparation, experiment protocols adopted, and the program established are described below.

3.1 Sample preparation

Materials were prepared according to the protocol presented in section 0. Samples were then compacted to the maximum dry density at the optimum water content by means of the static compaction method at a controlled deformation rate of 0.1 mm/s. The protocol envisaged the compaction of materials directly inside the mold in order to reduce the risk of the development of preferential paths along the sample/mold-interface. The initial height and diameter of all samples were 30 mm and 70 mm, respectively. Information about the initial characteristics of COX_c and mixture-samples is given in Table 3.

In the case of the mixture-samples, the microstructural and textural analyses were performed shortly after the termination of the hydraulic conductivity experiments. Before they were analyzed, samples were cut perpendicularly to their center axis into discs of same height. The center axis corresponded to the imposed flow direction. The purpose of this preparation

step was to determine the possible spatial evolution of the microstructure and texture triggered by the saturation and the solution chemistry. Supplementary COX_c- and mixture-samples were prepared in the same way to evaluate the impact of the partial material replacement and to compare the structure of material before and after saturation.

3.2 Hydraulic conductivity experiments

The setup of hydraulic conductivity experiments is depicted in Figure 2. The employed constant-volume hydraulic conductivity cell (rigid wall permeameter) was composed of its mold, two porous discs, its lid, and its bottom plate. The latter two included one o-ring each. The mold containing the sample was sandwiched between the porous discs. This assembly was then placed between the lid and the bottom part, which were finally screwed together.

The constant head method was considered to be most adequate to investigate the hydraulic conductivity of both samples (e.g. Dixon et al., 1999; Mata and Ledesma, 2003; Villar, 2006). By means of a constant volume/ pressure control unit, samples were saturated from the bottom upwards. Solutions left the cell at its top and were finally collected in a graduated flask. The accuracy of the measurement of outflow was about 0.5 mL. In order to avoid interaction processes of the solution with the atmosphere (e.g. evaporation, exchange of CO_2), the flask was plugged, allowing only solutions to enter. The increase of gas pressure inside the flask was expected to be negligible.

Imposed injection pressures increased stepwise from 15 kPa to 90 kPa in the first weeks of the experiments. Considering a sample height of 30 mm, corresponding hydraulic gradients varied from 50 m/m to 300 m/m, which reflected the conditions encountered in situ. The pore pressure measured in undisturbed COX-claystone varies from 4,000 to 5,000 kPa (Seyedi et al., 2017). Assuming atmospheric pressure in the drift and a minimum extension of the EdZ of about 8 m, the corresponding hydraulic gradient varies from 50 m/m to 60 m/m. Hydraulic gradients that were imposed in this experiment program were still higher since there was a need

to accelerate the experiments. The minimum volume injected was equal to two times of the initial pore volume of the sample.

Hydraulic conductivity experiments were performed under an ambient temperature of 22°C. The temperature was in accordance with the results of Tourchi et al. (2021), who reproduced a full-scale in situ heating experiment in COX-claystone by performing numerical simulations. Their simulations revealed that the temperature at the edge of the access galleries would not exceed 23°C after waste emplacement.

3.3 Microstructural analysis

Mercury intrusion porosimetry (MIP) experiments were conducted by means of an AutoPore IV 9500 apparatus (Micromeritics, U.S.A.). Prior to the microstructural analysis, samples were outgassed under a residual pressure of 1.6×10^{-6} Pa at a temperature of 80°C for 24 hours. The residual pressure involves the condensation of pore water at lower temperatures and, in turn, negligible shrinkage. Gaboreau et al. (2016) evaluated different pre-treatment methods for microstructural analysis and showed that the method adopted yields coherent results.

The MIP-method bases on the principle of forcing a non-wetting fluid, like mercury, to enter a porous medium by incrementally increasing injection pressures. Detailed information about its principle and procedure are given in Cuisinier and Laloui (2004) and Delage et al. (2006), for instance. The result of MIP-experiments is the cumulative volume of mercury intruded as a function of the equivalent pore diameter. The pore size distribution (PSD) curve is deduced from those results in order to facilitate their interpretation (Juang and Holtz, 1986). It is defined as the derivative of the total volume of mercury intruded with respect to the common logarithm of the equivalent pore diameter. In this study, the approach of PSD-curve determination followed that presented by Juang and Holtz (1986) and used a constant value of $\Delta(\log(d_i))$ being equal to 0.25. The determination of PSD by means of MIP is limited, regarding the intru-

sion of pores, whose diameter are smaller and larger than 7 nm and 600 nm, respectively. Results might also be impaired through the occurrence of the bottleneck phenomenon or pore entrapment, for instance (e.g. Romero et al., 1999; Delage et al., 2006; Romero, 2013).

3.4 Textural analysis

Nitrogen gas (N_2) adsorption-desorption cycles were determined by means of an ASAP 2050 volumetric adsorption analyzer (Micromeritics, U.S.A.) at 77K. Block samples were initially outgassed under a residual pressure of $1.6x10^{-6}$ Pa at 80°C. The outgassing lasted 24 hours. The nitrogen gas adsorption method adopts the physical adsorption of non-reactive gas molecules, like nitrogen, on solid external surfaces. Information about its principle and procedure is given in Gregg and Sing (1982), for instance. BET theory and a generalized *t*-plot method were adopted to describe the texture of solids (Lippens and Boer, 1965).

3.5 Pore classification

The diameter of macropores is larger than $5x10^1$ nm, whereas the diameter of mesopores ranges between $2x10^0$ nm and $5x10^1$ nm. Micropores are characterized by a diameter smaller than $2x10^0$ nm (e.g. Thommes et al., 2015). In this study, the lower limit of the class of mesopores was shifted to the entrance pore diameter of $7x10^0$ nm, since the mesopores, whose diameters are smaller than $7x10^0$ nm, cannot be detected by means of the MIP method. The range of the class of mesopores was accordingly reduced by 10% and the bias was expected to be negligible in the further interpretation of results.

3.6 Experimental program

The program comprised four samples of COX_c and four samples of the mixture, respectively indicated by the prefix C and M in their sample identification. The suffix I, W, SS and AS referred to samples analyzed in their initial state, and to samples analyzed during/ after the

saturation with water, site solution and alkaline solution, respectively. The detailed experiment program is given in Table 4. In terms of structural alterations, M-SS and M-AS were expected to react most considerably to the saturation with different solutions due to their elevated smectite fraction and particular solution chemistry. Therefore, they were selected for the subsequent microstructural and textural analysis. This approach provided the basis to evaluate the impact of the saturation process and saturating solution chemistry on the material properties.

4 Results

In this section, the results obtained in the hydraulic conductivity experiments are presented first, followed by the results of subsequent microstructural and textural analysis. The presentation reflects the sequence of data acquisition.

4.1 Hydraulic conductivity experiments

Values of hydraulic conductivity were determined upon the establishment of steady state condition (hydraulic equilibrium) that was indicated by stabilized rates of inflow and outflow of solutions. Moreover, the hydraulic equilibrium implied full saturation of samples. Both materials were saturated with water, the site and alkaline solution. The normalized volume of inflow and the hydraulic conductivity of COX_c are plotted against the normalized volume of outflow in Figure 3a and c, respectively, whereas Figure 3b and d depict the evolution of the normalized volume of inflow and hydraulic conductivity of the mixture as a function of the normalized volume of outflow. The normalized volume of inflow and outflow are the ratios of volume of measured inflow and outflow, respectively, to the initial pore volume and serves the purpose of emphasizing the amount of pore solution exchanged. Data obtained were subsequently processed by means of a moving average method.

Focusing on COX_c, inflow rates increased once the hydraulic gradient was raised stepwise and stabilized. The inflow volume ranged from the threefold to the fivefold of the initial pore

volume. The greatest volume of solution was injected into C-AS. In all three experiments, the onset of outflow was determined once the volume of solution corresponding to one initial pore volume was injected into the samples. Shortly after the onset of outflow was detected, steady state conditions established at an average flow rate ranging from 2 mL/day to 2.5 mL/ day. The former rate refers to C-W. As depicted in Figure 3a and c, pore solution was exchanged at least twice within a period of about 60 days. The smallest number of exchanges was exhibited by C-W, which corresponded to the smaller average flow rates. In the course of the experiments, values of hydraulic conductivity calculated decreased initially and stabilized at values between $6x10^{-11}$ m/s to $9x10^{-11}$ m/s. Samples C-SS and C-AS exhibited slightly higher hydraulic conductivities than C-W.

Total inflow volume into mixture-samples varied from the twofold to the threefold of the initial pore volume and were thus less than that injected into COX_c-samples, despite the fact that the experiments lasted five to six times longer (300 days – 360 days). In the case of M-W and M-SS, outflow was detected after injecting the volume of solution corresponding to one initial pore volume. In the case of M-AS, the volume of solution corresponding to two initial pore volumes were injected prior to the onset of outflow that might be attributable to a greater amount of air in the porous disc of the bottom plate. Indeed, steady state conditions were established shortly after detecting an outflow. However, the inflow and outflow rates decreased steadily in the course of the experiments, starting from 0.4 mL/ day at the beginning to 0.2 mL/ days in the end. The trend is also identifiable in Figure 3d. Values of hydraulic conductivity accordingly decreased from $2x10^{-11}$ m/s to $3x10^{-12}$ m/s. Comparing the values of hydraulic conductivity at the same normalized outflow of 0.6, M-AS exhibited the smallest values.

The hydraulic conductivity of COX_c was by one order of magnitude higher than that of the mixture. The difference became even more considerable as the values of COX_c stabilized, whereas the values of the mixture progressively decreased in the course of the experiment.

Apart from that, the chemistry of the site and alkaline solution had no considerable impact on the hydraulic conductivity of both materials. The characterization of the microstructure and texture was of special interest at this stage, in order to evaluate whether the evolution at macroscale was reflected in the material properties at the nano- and microscale.

4.2 Microstructural analysis

Samples were prepared by cutting them perpendicularly to their center axis into two discs of same height (15 mm) in the case of MIP experiments. Henceforth, top part (T) and bottom part (B) referred to the upper part and lower part of the initial sample, respectively. Results of MIP-experiments performed on C-I, M-I, M-SS and M-AS are depicted in Figure 4.

In general, the quantities of micropores, mesopores and macropores are expressed as micro-void ratio (e_μ), meso-void ratio (e_m) and macro-void ratio (e_M), respectively. The cumulative void ratio was calculated as the ratio of the cumulated volume of mercury intruded in voids to the volume of solids. The micro-void ratio was defined as the difference between the total void ratio (e_{Tot}) and the sum of the meso-void ratio and the macro-void ratio. Since the porosity (n) of top and bottom parts of each sample was also measured in MIP-experiments, the total void ratio (e_{Tot}) was calculated as the ratio of porosity to the difference of 1 to porosity. The approach was exemplified by the top parts of samples in Figure 4. Complementing Figure 4, Table 5 provides absolute and relative values of micro-, meso-, and macro-void ratios. It facilitates the evaluation of the impact of partial replacement of COX_c by MX80-bentonite, saturation and solution chemistry. Relative values were defined as the ratios of micro-, meso-, and macro-void ratio to the total void ratio of the corresponding sample part (= normalization) and are provided in order to disregard the impact of initial dry density, in particular on the macro-void ratios.

In the case of C-I, the volume of pores appeared to reduce along the center axis of the sample since the cumulative volume of mercury intruded in C-I (T) was higher than that of C-I (B). In the case of M-I, the opposite was observed. A distinct double peak was revealed by

374 the pore size distribution curves in the upper parts of Figure 4. It indicated the existence of
375 meso- and macropores. As depicted in Figure 4a, the peaks of meso- and macropores of C-I (T)
376 and C-I (B) occurred at the same pore diameter of about $4x10^1$ nm and $2.5x10^4$ nm, respec-
377 tively. The comparison of relative meso- and macro-void ratios of C-I (T) to those of C-I (B)
378 revealed similar values. M-I (T) was characterized by meso- and macropores at pore diameters
379 of about $3x10^1$ nm and $5x10^4$ nm, respectively (Figure 4c). Meso- and macropores of M-I (B)
380 occurred at pore diameters of about $4x10^1$ nm and $2.5x10^4$ nm, respectively. The relative meso-
381 void ratio of M-I (T) was 5% higher than that of M-I (B), whereas the relative macro-void ratio
382 of M-I (T) was 8% lower than that of M-I (B).

383 As highlighted in the lower parts of Figure 4 and in Table 5, the microstructure of M-SS
384 and M-AS evolved comparably, despite they were saturated with different solutions. Top parts
385 of M-SS and M-AS were characterized by the majority of mesopores occurring at a diameter
386 of $2.5x10^1$ nm. Compared to those of M-I (T), relative meso-void ratios of M-SS (T) and
387 M-AS (T) increased by 7% and 9%, respectively. The majority of macropores was determined
388 at a diameter of $4x10^4$ nm in the cases of M-I (T) and M-AS (T), and at a diameter of $2x10^4$ nm
389 in the case of M-SS (T). The comparison of the relative macro-void ratio of M-I (T) to those of
390 M-SS (T) and M-AS (T) revealed similar values. M-AS (B) was characterized by a mesopore
391 diameter of $2x10^1$ nm, whereas the mesopores of M-SS (B) occurred at $4x10^1$ nm. Relative
392 meso-void ratios of both M-SS (B) and M-AS (B) were increased by about 8% and 15%, re-
393 spectively, when they are compared to M-I (B). Bottom parts of mixture samples were charac-
394 terized by the majority of macropores occurring at a diameter of $2x10^4$ nm. Interestingly, an
395 additional macropore population was determined at diameters of $8x10^4$ nm in the case of
396 M-SS (B). Compared to those of M-I (B), relative macro-void ratios of M-SS (B) and M-AS (B)
397 reduced by about 9% and 6%, respectively.

The similar relative micro-, meso- and macro-void ratios of C-I and M-I accounted for the fact that the impact of the partial replacement of COX_c by MX80-bentonite remained unclear yet. Unlike the solution chemistry, the saturation had an impact on the microstructure of samples since the relative micro- and macro-void ratios decreased and aligned with each other, and the relative meso-void ratios increased.

4.3 Textural analysis

In the case of textural analysis, sample preparation involved to cut samples perpendicularly to their center axis into three discs of same height (10 mm) in order to identify possible spatial variations in the N_2-gas sorption isotherms and the external specific surface area (SSA) along the flow direction. Henceforth, top part (Top), middle part (Middle) and bottom part (Bottom) referred to the upper, middle and lower parts of the initial sample, respectively. Sorption isotherms determined by means of the N_2-gas sorption method are depicted in Figure 5.

Isotherms displayed a Type II behavior and a H3 hysteresis loop. The reversible Type II isotherm is the normal form of isotherm obtained with a macroporous adsorbent. The Type II represents unrestricted multilayer adsorption build up and the occurrence of mesopores. The Type H3 loop not exhibiting any limited adsorption at high P/P_0-ratios was coherent with aggregates of plate-like particles. It gave rise to slit-shaped pores and proved that the samples were mesoporous. Isotherms gave linear BET plots from 0.04 to 0.4 P/P_0 for all tested samples.

SSA-values obtained by means of BET- and *t*-plot-method are compiled in Table 6. Calculated BET specific surface areas (S_{BET}) and associated monolayer capacity (V_m) exhibited neither variations in SSA among mixture-samples, nor an evolution of SSA over the length of the individual samples. *t*-plot results were coherent with the S_{BET}- values.

5 Discussion

The study aimed to understand the evolution of hydraulic conductivity of COX_c and its mixture with MX80-bentonite under quasi-realistic conditions by relating the results obtained at the macroscale to those obtained at the microscale. Quasi-realistic conditions refer to the fact that the compaction conditions, solution chemistry, ambient temperature and hydraulic gradient were believed to be in a realistic range. Since the saturation itself as well as the saturation with solutions of different chemistry affected the materials in more or less pronounced manner, it appeared to be suitable to arrange the discussion accordingly.

5.1 Impact of saturation

The existence of meso- and macropores in COX_c and its mixture with MX80-bentonite was indicated by bi-modal PSD-curves. This finding was consistent with the literature as smectite-containing materials are usually characterized by such a double-structure if they are compacted at the dry side of optimum water content (Alonso et al., 1987).

Highlighted in Table 5, the void ratio of M-I (T) was lower than that of M-I (B). The density gradient was induced by the static compaction method and ensued as a shear stress evolved at the interface between the material and mold (e.g. Villar, 2006). The decrease in initial dry density raised the total pore volume, in particular the macropore volume. This finding was consistent with the literature (e.g. Lloret and Villar, 2007). Interestingly, the static compaction method had no impact on the distribution of pores in C-I (T) and C-I (B), although its water content was smaller than that of M-I. As a consequence, the evolution of higher shear stresses and a density gradient was expected.

The normalization of void ratios allowed to disregard the impact of densification on the microstructure of C-I and M-I and to evaluate quantitatively the impact of the partial replacement of COX_c by MX80-bentonite. The comparison of C-I to M-I indicated that M-I indeed incorporated more macro-pores but less meso-pores on average. The average micro-void ratios

445 of C-I and M-I were comparable (Table 5). Apparently, the higher macro-void ratio of M-I
446 ensued as the higher amount of smectite particles provoked the formation of more card-house-
447 like aggregates, including more inter-aggregate pores.

448 The saturation of M-SS and M-AS led to a decrease in macro-void ratios and to an in-
449 crease in micro- and meso-void ratios. Small differences along the center axis likely indicated
450 a homogeneous saturation of samples. The decrease in macro-void ratio was attributable to the
451 closure of hydraulic conductive pores ensuing as smectite particles and aggregates swell and
452 rearrange upon saturation (e.g. Komine, 2004, 2010).

453 Information about COX_c and its mixtures with MX80-bentonite, in particular their one-
454 dimensional compression and swelling behavior under saturation, is given by Tang et al. (2010),
455 Wang et al. (2012), Zeng et al. (2019), Middelhoff et al. (2020) and Robinet et al. (2021), for
456 instance. In contrast, their hydraulic conductivity behavior under saturation was less intensely
457 analyzed. The studies of Zhang and Kröhn (2019) and Zhang (2021) were thus of major interest
458 since they determined the saturated hydraulic conductivity of compacted COX_c and different
459 COX_c/ MX80-bentonite-mixtures, among other hydro-mechanical parameters. Prior to testing,
460 all samples of Zhang and Kröhn (2019) were prepared to target dry densities of about 2.0 Mg/m^3
461 at initial water contents of about 4%. The corresponding total void ratios were about 0.33. In
462 the case of COX_c, values of hydraulic conductivity were about $5x10^{-13}$ m/s and assumed to
463 reflect a long-term stable state. Tang et al. (2010) also focused on the saturated hydraulic con-
464 ductivity of COX_c, whose initial water contents ranged between 2% to 8%. Target dry densities
465 were also about 2.0 Mg/m^3. They determined a saturated hydraulic conductivity of about $3x10^{-12}$ m/s. Moreover, their results indicated to a negligible impact of the initial water content on
467 the hydraulic conductivity. The one and two orders of magnitude lower saturated hydraulic
468 conductivities of Tang et al. (2010) and Zhang and Kröhn (2019) were attributable to the lower
469 initial dry densities and/ or higher initial total void ratios of C-SS and C-AS most probably

(Table 5). In the case of a mixture that was composed of 80% COX_c and 20% MX80-bentonite in weight, Zhang and Kröhn (2019) measured values of saturated hydraulic conductivities varying from $1x10^{-12}$ m/s to 2 $x10^{-12}$ m/s. Their values were in good agreement with the values obtained for M-SS and M-AS. Considering the initial compaction conditions, the recent results were remarkable since Zhang and Kröhn (2019) and Zhang (2021) compacted mixture samples to higher initial dry densities at lower initial water content with higher compaction energy before they performed hydraulic conductivity experiments. Nevertheless, the magnitude of saturated hydraulic conductivities was the same ($x10^{-12}$ m/s). This comparison highlighted the efficiency of the rearrangement of hydraulic conductive macropores ensuing as the smectite fraction swells upon its saturation. Further, it accounted for the difference in the performance of COX_c and its mixture with MX80-bentonite.

As the values of hydraulic conductivity progressively decreased, it was hypothesized that the microstructure in COX_c/ MX80-bentonite-mixture samples was still rearranging after more than one year of saturation, and that values of hydraulic conductivities were likely reflecting a short- or intermediate-term state. In order to corroborate the hypothesis, the kinetics of hydraulic conductivity experiments were compared to that of constant-volume swelling pressure experiments of Middelhoff et al. (2020). They performed those experiments on similar samples under comparable conditions and observed the establishment of constant swelling pressure after seven days of saturation. The different kinetics was attributed to the hydraulic gradient exceeding 500 m/m in constant-volume swelling pressure experiments. The higher hydraulic gradient involved higher rates of normalized inflow, thus a greater volume of solution for hydro-mechanical processes was accessible in less time. This might account for an accelerated kinetics in constant-volume swelling pressure experiments. Nevertheless, it is recommendable to per-

493 form combined constant-volume swelling pressure/ constant-head hydraulic conductivity ex-
494 periments in order to better understand the kinetics of swelling pressure build-up and swelling-
495 induced pore closure and their coupling.

496 5.2 Impact of solution chemistry

497 The texture and microstructure of M-SS and M-AS were more affected by the saturation
498 than by the solution chemistry. The solution chemistry, in particular that of the alkaline solution,
499 had no impact neither on the shape of N_2-gas sorption isotherms nor on SSA-values nor on their
500 spatial distribution (e.g. Figure 5). Considerable textural and microstructural changes were ex-
501 pected as the alkaline solution percolates the materials over time and dissolve the clay minerals
502 therein. In turn, their dissolution alters the shape of mesopores and increases the fraction of
503 macropores (Karnland et al., 2007; Cuisinier et al., 2008; Cuisinier et al., 2014). The impact of
504 the solution chemistry must be considered to be highly time-dependent. The reaction kinetics
505 appeared to be low under realistic conditions, and dissolution processes presumably did not
506 come into effect, yet.

507 There was no considerable impact of the solution chemistry on the hydraulic conductivity
508 behavior exhibited by M-W and M-SS. It might be attributable to the low ionic strength of the
509 site solution (I_{SS} = 105 mmol/L). According to the theories of diffuse double layers (DDL), the
510 solution chemistry has an impact on the hydraulic conductivity behavior of smectite-based ma-
511 terials, when diffuse double layers evolve in macropores and immobilize water molecules
512 therein. The ion concentration in solution is inversely proportionally related to their layer thick-
513 ness. An increase in hydraulic conductivity ensues as the ion concentration increases and, in
514 turn, diffuse double layers diminish (e.g. Dixon, 2000; Villar, 2006; Castellanos et al., 2008).

515 In contrast, M-AS exhibited lowest values of hydraulic conductivity at the same normal-
516 ized outflow of 0.6. This might be attributable to the clogging of hydraulic conductive
517 macropores through swelling as well as precipitation of $Ca(OH)_2$. The majority of pores in

M-AS were initially filled with water. Upon saturation, the pH-value of the alkaline solution dropped as it mixed with the pore water, and the consequent precipitation of $Ca(OH)_2$ intensified the clogging of macropores. $Ca(OH)_2$ precipitated until the alkaline solution determined the pH-value of the pore solution, and dissolved then again. Since the precipitation of $Ca(OH)_2$ changes the texture of materials, in particular their SSA-values, but N_2-gas sorption analyses revealed no changes, it can be hypothesized that $Ca(OH)_2$ already dissolved at that stage. An analyzes of the effluent and comparison of its $Ca(OH)_2$-content to that of the influent can corroborate the hypothesis. Considering Middelhoff et al. (2020), the precipitation of $Ca(OH)_2$ presumably has no impact on the evolution of swelling pressure, unlike on that of hydraulic conductivity.

Apart from the low reaction kinetics under imposed conditions, the low volume of pore solution exchanged might account for the apparently negligible impact of the solution chemistry. As shown in Figure 3b, pore solution was exchanged less than once. Geochemical reactions, in particular dissolution and precipitation processes, appeared to not come into effect yet, despite the experiment duration of more than 300 days. The adoption of a different termination criteria is thus recommended that additionally considers the composition, ionic strength, and electric conductivity of the influent and effluent in order to predict the initiation of geochemical reactions in the course of the experiment more precisely. For instance, Jo et al. (2005) carried out long-term hydraulic conductivity experiments on geosynthetic clay liners. Values of hydraulic conductivity were measured once hydraulic equilibrium established and once both hydraulic and chemical equilibrium established. Unlike the former, the latter criteria was not met until the pore solution was exchanged several times. The comparison of results revealed an underestimation of the hydraulic conductivity by a factor of two when the termination criteria relied on the hydraulic equilibrium criteria exclusively. This also highlights the importance of volume of pore solution exchanged.

6 Conclusions

Crushed Callovo-Oxfordian claystone (COX_c) and a mixture composed of 70% COX_c and 30% MX80-bentonite in weight might be employed to backfill drifts and shafts of a future nuclear waste repository located in deep sedimentary rock formations. In addition to the swelling pressure, the hydraulic conductivity is one of the key parameters determining the performance of the backfill. This study aimed to understand the evolution of the hydraulic conductivity by means of laboratory experiments, whose boundary conditions were believed to portray the real conditions in terms of compaction conditions, solution chemistry, temperature and hydraulic gradient. Subsequently conducted microstructural and textural analysis allowed to relate the evolution of the hydraulic conductivity at the macroscale to changes at the microscale possibly affected by the solution chemistry, in particular the pH-value. Following major conclusions can be drawn for COX_c and its mixture with MX80-bentonite:

1. The microstructural analysis showed considerable microstructural rearrangements, which were related to closure of macropores triggered by material swelling upon saturation. The interpretation was consistent with the observations and the literature. The negligible impact of the solution chemistry was attributed to the low volume of exchanged pore solution under imposed conditions.
2. In the case of COX_c and the mixture, values of hydraulic conductivity were in good agreement with the literature. COX_c exhibited stabilized values of hydraulic conductivity soon upon establishing steady state conditions. Conversely, values of hydraulic conductivity of the mixture progressively decreased in the course of the experiment. Considering the results of microstructural analysis, the closure of hydraulic conductive macropores through material swelling upon saturation likely accounted for the evolution of the hydraulic conductivity on the one side and for the difference in the performance of COX_c and the mixture on the other side. The duration of some experiments was longer than one

year and highlighted the low kinetics of geochemical reactions under the imposed conditions. Hence, the hydraulic conductivity appeared to be little affected by the solution chemistry within one year of experiment duration. In order to study the time-dependent impact of solution chemistry more precisely, it is of major interest to conduct experiments which involve the exchange of several volumes of pore solution.

This study revealed that the replacement of COX_c by 30% MX80-bentonite in weight enhanced considerably the barrier functions of compacted backfill materials under realistic conditions in terms of their short- and intermediate-term hydraulic conductivity. The enhancement can be attributed to the more effective clogging of hydraulic conductive voids. However, important questions arose while evaluating the experiments. For instance, it is still unclear how the hydraulic conductivity evolves under imposed conditions in long-term, particularly with regard to the time-dependent impact of the solution chemistry that must not be considered as negligible and of the consolidation of the backfill material induced by the convergence of the rock formation.

Declaration of interest

The authors wish to confirm that there are no known conflicts of interest associated with this publication and there has been no significant financial support for this work that could have influenced its outcome.

Funding

The work presented in this paper has been carried out during the preparation of the PhD thesis of the first author, which is funded by Andra (France), the French agency in charge of the management and disposal of nuclear waste.

Acknowledgement

The authors thank Dr. F. Claret of BRGM and Dr. G. Armand of Andra for fruitful discussions that helped to improve this article. Moreover, the authors gratefully thank the two anonymous reviewers for their rigorous revisions.

7 References

Alonso, E.E., Gens, A., Whight, D.W., 1987. General Report, in: Groundwater effects in geotechnical engineering. Ninth european conference on soil mechanics and foundation engineering, Dublin. 31.08. - 03.09. A. A. Balkema, Rotterdam, Brookfield, pp. 1087–1146.

ANDRA, 2005. Dossier 2005 Argile Synthesis: Evaluation of the feasibility of a geological repository in an argillaceeous formation. Meuse/ Haute-Marne site. Collection les Rapports. Agence nationale pour la gestion des déchets radioactifs, Châtenay-Malabry, 1497 pp.

Burland, J.B., 1990. On the compressibility and shear strength of natural clays. Géotechnique 40, 329–378.

Castellanos, E., Villar, M.V., Romero, E., Lloret, A., Gens, A., 2008. Chemical impact on the hydro-mechanical behaviour of high-density FEBEX bentonite. Physics and Chemistry of the Earth, Parts A/B/C 33, S516-S526.

Chen, F.H., 1988. Foundations on expansive soils. Elsevier science pub, Amsterdam, New York, 1463 pp.

Conil, N., Talandier, J., Djizanne, H., La Vaissière, R. de, Righini-Waz, C., Auvray, C., Morlot, C., Armand, G., 2018. How rock samples can be representative of in situ condition: A case study of Callovo-Oxfordian claystones. Journal of Rock Mechanics and Geotechnical Engineering 10, 613–623.

Cuevas, J., 2005. Geochemical reactions in FEBEX bentonite. In: Michau, N. (Ed.) ECOCLAY II - Effects of cement on clay barrier performance. Phase II. Final report, pp. 105–117.

Cuisinier, O., Deneele, D., Masrouri, F., Abdallah, A., Conil, N., 2014. Impact of high-pH fluid circulation on long term hydromechanical behaviour and microstructure of compacted clay from the laboratory of Meuse-Haute Marne (France). Applied Clay Science 88-89, 1–9.

Cuisinier, O., Laloui, L., 2004. Fabric evolution during hydromechanical loading of a compacted silt. International Journal for Numerical and Analytical Methods in Geomechanics 28, 483–499.

Cuisinier, O., Masrouri, F., Pelletier, M., Villieras, F., Mosser-Ruck, R., 2008. Microstructure of a compacted soil submitted to an alkaline PLUME. Applied Clay Science 40, 159–170.

Delage, P., Marcial, D., Cui, Y.J., Ruiz, X., 2006. Ageing effects in a compacted bentonite: a microstructure approach. Géotechnique 56, 291–304.

Dixon, D.A., 2000. Porewater salinity and the development of swelling presure in bentonite-based buffer and backfill materials 2000-04. POSIVA Oy, Helsinki, 51 pp. Accessed 27 October 2019.

Dixon, D.A., Graham, J., Gray, M.N., 1999. Hydraulic conductivity of clays in confined tests under low hydraulic gradients. Canadian Geotechnical Journal 36, 815–825.

Elert, K., Pardo, E., Rodriguez-Navarro, C., 2015. Mineralogical Evolution of Di- and Trioctahedral Smectites in Highly Alkaline Environments. Clays and Clay Minerals 63, 414–431.

Fernández, R., Ruiz, A.I., Cuevas, J., 2014. The role of smectite composition on the hyperalkaline alteration of bentonite. Applied Clay Science 95, 83–94.

Gaboreau, S., Lerouge, C., Dewonck, S., Linard, Y., Bourbon, X., Fialips, C.I., Mazurier, A., Prêt, D., Borschneck, D., Montouillout, V., Gaucher, E., Claret, F., 2012. In-situ interaction of cement paste and shotcrete with claystones in a deep disposal context. American Journal of Science 312, 314–356.

642 Gaboreau, S., Prêt, D., Tinseau, E., Claret, F., Pellegrini, D., Stammose, D., 2011. 15 years of
643 in situ cement–argillite interaction from Tournemire URL: Characterisation of the multi-
644 scale spatial heterogeneities of pore space evolution. Applied Geochemistry 26, 2159–
645 2171.
646 Gaboreau, S., Robinet, J.-C., Prêt, D., 2016. Optimization of pore-network characterization of
647 a compacted clay material by TEM and FIB/SEM imaging. Microporous and Mesoporous
648 Materials 224, 116–128.
649 Gaucher, E., Robelin, C., Matray, J.M., Négrel, G., Gros, Y., Heitz, J., Vinsot, A., Rebours,
650 H., Cassagnabère, A., Bouchet, A., 2004. ANDRA underground research laboratory: inter-
651 pretation of the mineralogical and geochemical data acquired in the Callovian–Oxfordian
652 formation by investigative drilling. Physics and Chemistry of the Earth, Parts A/B/C 29,
653 55–77.
654 Gregg, S.J., Sing, K.S., 1982. Adsorption, surface area and porosity, 2nd ed. Academic Press,
655 London, New York.
656 Herbert, H.-J., Kasbohm, J., Moog, H., Henning, K.-H., 2004. Long-term behaviour of the
657 Wyoming bentonite MX-80 in high saline solutions. Applied Clay Science 26, 275–291.
658 Herbert, H.-J., Kasbohm, J., Sprenger, H., Fernández, A.M., Reichelt, C., 2008. Swelling
659 pressures of MX-80 bentonite in solutions of different ionic strength. Physics and Chemis-
660 try of the Earth, Parts A/B/C 33, S327-S342.
661 Hofmann, H., Bauer, A., Warr, L.N., 2004. Behavior of Smectite In Strong Salt Brines Under
662 Conditions Relevant to the Disposal of Low- to Medium-grade Nuclear Waste. Clays and
663 Clay Minerals 52, 14–24.
664 Huertas, F., Farias, J., Griffault, L., Leguey, S., Cuevas, J., Ramírez, S., Vigil de la Villa, R.,
665 Cobena, J., Andrade, C., Alonso, M.C., Hidalgo, A., Parneix, J.C., Rassineux, F., Bouchet,

A., Meunier, A., Decarreau, S., Petit, S., Vieillard, P., 2000. ECOCLAY I - Effects of cement on clay barrier performance. Final report. Off. for Off. Publ. of the Europ. Communities, Luxembourg, 140 pp.

ISO, 2009. Particle size analysis: Laser diffraction methods.

Jo, H.Y., Benson, C.H., Shackelford, C.D., Lee, J.-M., Edil, T.B., 2005. Long-Term Hydraulic Conductivity of a Geosynthetic Clay Liner Permeated with Inorganic Salt Solutions. J. Geotech. Geoenviron. Eng. 131, 405–417.

Juang, C.H., Holtz, R.D., 1986. A probabilistic permeability model and the pore size density function. International Journal for Numerical and Analytical Methods in Geomechanics 10, 543–553.

Karnland, O., Olsson, S., Nilsson, U., Sellin, P., 2007. Experimentally determined swelling pressures and geochemical interactions of compacted Wyoming bentonite with highly alkaline solutions. Physics and Chemistry of the Earth, Parts A/B/C 32, 275–286.

Komine, H., 2004. Simplified evaluation on hydraulic conductivities of sand–bentonite mixture backfill. Applied Clay Science 26, 13–19.

Komine, H., 2010. Predicting hydraulic conductivity of sand–bentonite mixture backfill before and after swelling deformation for underground disposal of radioactive wastes. Engineering Geology 114, 123–134.

Krauskopf, K.B., 1956. Dissolution and precipitation of silica at low temperatures. Geochemica et Cosmochemica Acta 10, 1–26.

Lippens, B., Boer, J.H. de, 1965. Studies on pore systems in catalysts V. The t method. Journal of Catalysis 4, 319–323.

Lloret, A., Villar, M.V., 2007. Advances on the knowledge of the thermo-hydro-mechanical behaviour of heavily compacted “FEBEX” bentonite. Physics and Chemistry of the Earth, Parts A/B/C 32, 701–715.

691 Mata, C., 2003. Hydraulic behavior of bentonite based mixtures in engineered barriers: The
692 backfill and plug test at the Aespoe HRL (Sweden). PhD Thesis, Barcelona, 280 pp.
693 Mata, C., Ledesma, A., 2003. Permeability of a bentonite-crushed granite rock mixture using
694 different experimental techniques. Géotechnique 53, 747–758.
695 Michau, N. (Ed.), 2005. ECOCLAY II - Effects of cement on clay barrier performance: Phase
696 II. Final report, 378 pp.
697 Middelhoff, M., Cuisinier, O., Masrouri, F., Talandier, J., Conil, N., 2020. Combined impact
698 of selected material properties and environmental conditions on the swelling pressure of
699 compacted claystone/bentonite mixtures. Applied Clay Science 184, 105389.
700 Molinero-Guerra, A., Delage, P., Cui, Y.J., Mokni, N., Tang, A.M., Aimedieu, P., Bernier, F.,
701 Bornert, M., 2020. Water-retention properties and microstructure changes of a bentonite
702 pellet upon wetting/drying; application to radioactive waste disposal. Géotechnique 70,
703 199–209.
704 Norrish, K., 1954. The swelling of montmorillonite. Discuss. Faraday Soc. 18, 120.
705 Orsini, L., Remy, J.C., 1976. Utilisation du chlorure de cobaltihexammine pour la détermina-
706 tion simultanée de la capacité d'échange et des bases échangeables des sols. Bulletin de
707 l'AFES Science du Sol 4, 269–275.
708 Pusch, R., Zwahr, H., Gerber, R., Schomburg, J., 2003. Interaction of cement and smectitic
709 clay—theory and practice. Applied Clay Science 23, 203–210.
710 Ramírez, S., Vieillard, P., Bouchet, A., Cassagnabère, A., Meunier, A., Jacquot, E., 2005. Al-
711 teration of the Callovo–Oxfordian clay from Meuse-Haute Marne underground laboratory
712 (France) by alkaline solution. I. A XRD and CEC study. Applied Geochemistry 20, 89–99.
713 Robinet, J.-C., Tyri, D., Djeran-Maigre, I., 2021. Hydro-mechanical response of crushed ar-
714 gillite and bentonite mixtures as sealing material. Engineering Geology 288, 106140.

715 Romero, E., 2013. A microstructural insight into compacted clayey soils and their hydraulic
716 properties. Engineering Geology 165, 3–19.
717 Romero, E., Gens, A., Lloret, A., 1999. Water permeability, water retention and microstruc-
718 ture of unsaturated compacted Boom clay. Engineering Geology 54, 117–127.
719 Seyedi, D.M., Armand, G., Noiret, A., 2017. "Transverse Action" – A model benchmark ex-
720 ercise for numerical analysis of the Callovo-Oxfordian claystone hydromechanical re-
721 sponse to excavation operations. Computers and Geotechnics 85, 287–305.
722 Tang, C.S., Tang, A.M., Cui, Y.J., Delage, P., Shi, B., 2010. The coupled hydro-mechanical
723 behaviours of compacted crushed Callovo-Oxfordian argillite. Journal of Rock Mechanics
724 and Geotechnical Engineering, 86–90.
725 Thommes, M., Kaneko, K., Neimark, A.V., Olivier, J.P., Rodriguez-Reinoso, F., Rouquerol,
726 J., Sing, K.S., 2015. Physisorption of gases, with special reference to the evaluation of sur-
727 face area and pore size distribution (IUPAC Technical Report). Pure and Applied Chemis-
728 try 87, 1051–1069.
729 Tourchi, S., Vaunat, J., Gens, A., Bumbieler, F., Vu, M.-N., Armand, G., 2021. A full-scale in
730 situ heating test in Callovo-Oxfordian claystone: observations, analysis and interpretation.
731 Computers and Geotechnics 133, 104045.
732 Villar, M.V., 2006. Infiltration tests on a granite/bentonite mixture: Influence of water salin-
733 ity. Applied Clay Science 31, 96–109.
734 Wang, Q., Cui, Y.J., Delage, P., Gatmiri, B., 2012. Experimental study on the swelling behav-
735 iour of bentonite/claystone mixture. Engineering Geology 124, 59–66.
736 Ye, W.M., Zheng, Z.J., Chen, B., Chen, Y.G., Cui, Y.J., Wang, J., 2014. Effects of pH and
737 temperature on the swelling pressure and hydraulic conductivity of compacted GMZ01
738 bentonite. Applied Clay Science 101, 192–198.

739 Yven, B., Sammartino, S., Geraud, Y., Villieras, F., 2007. Mineralogy, texture and porosity of
740 Callovo-Oxfordian argillites of the Meuse/ Haute-Marne region eastern Paris Basin). Bul-
741 letin de la Societe Geologique de France, 73–90.
742 Zeng, Z., Cui, Y.J., Zhang, F., Conil, N., Talandier, J., 2019. Investigation of swelling pres-
743 sure of bentonite/claystone mixture in the full range of bentonite fraction. Applied Clay
744 Science 178, 105137.
745 Zhang, C.-L., 2021. Deformation and water/gas flow properties of claystone/bentonite mix-
746 tures. Journal of Rock Mechanics and Geotechnical Engineering 13, 864–874.
747 Zhang, C.-L., Kröhn, K.-P., 2019. Sealing behaviour of crushed claystone–bentonite mixtures.
748 Geomechanics for Energy and the Environment 17, 90–105.

749 Table 1: Physical and physico-chemical characteristics of COX_c, MX80-bentonite and the mixture

	Initial water content	Liquid limit	Plastic limit	Specific gravity	Cation exchange cap.	Ext. specific surface area
	w_{ini}	LL	PL	G_s	CEC	SSA
	[%]	[%]	[%]	[-]	[meq/100g]	[m²/g]
COX_c	5.4	37.3	24.9	2.68	22	37
Mixture	6.4	112.5	34.7	2.64	39	32

750

751 Table 2: Major compounds and properties of site solution and alkaline solution (Middelhoff et al., 2020)

	Na^+	K^+	Ca^{2+}	Mg^{2+}	Cl^-	HCO_3^-	SO_4^{2-}	OH^-	IS	pH
	[mmol/L]	[mmol/L]	[mmol/L]	[mmol/L]	[mmol/L]	[mmol/L]	[mmol/L]	[mmol/L]	[mmol/L]	[-]
SS	44.8	0.5	5.3	8.5	35.3	1.5	1.8	-	105	7.8
AS	22.1	8.0	19.0	-	30.1	-	-	38.1	87	12.5

SS: Site solution; AS: Alkaline solution; IS: Ionic strength

752

753 Table 3: Initial characteristics of employed samples

Material	Initial dry density	Initial water content	Initial void ratio	Initial porosity	Initial degree of saturation	Initial suction
	$\rho_{d,\,ini}$	w_{ini}	e_{ini}	n_{ini}	S_r	s
	[Mg/m^3]	[%]	[-]	[-]	[-]	[MPa]
COX_c	1.95	13.2	0.37	0.27	0.96	1.5
Mixture	1.72	18.2	0.53	0.35	0.91	2.7

754

755 Table 4: Experiment program including hydraulic conductivity experiments, microstructural and textural analysis

Sample ID.	C-I	C-W	C-SS	C-AS	M-I	M-W	M-SS	M-AS
Material	COX_c	COX_c	COX_c	COX_c	Mixture	Mixture	Mixture	Mixture
Solution	-	Water	SS	AS	-	Water	SS	AS
Constant head experiment	-	✓	✓	✓	-	✓	✓	✓
Mercury Intrusion Porosimetry (MIP)	✓	-	-	-	✓	-	✓	✓
N_2-gas sorption	✓	-	-	-	✓	-	✓	✓

✓: Experiment performed

756

757 Table 5: Absolute and relative values of microstructural characteristics of top and bottom parts of C-I, M-I, M-SS
758 and M-AS

	Absolute					Relative		
Sample-ID.	n*	e_{tot}	e_M	e_m	e_μ	e_M/e_{tot}	e_m/e_{tot}	e_μ/e_{tot}
	[-]	[-]	[-]	[-]	[-]	[-]	[-]	[-]
C-I (T)	0.28	0.388	0.225	0.111	0.052	0.58	0.29	0.13
C-I (B)	0.27	0.368	0.209	0.112	0.047	0.57	0.30	0.13
M-I (T)	0.34	0.501	0.287	0.146	0.068	0.57	0.29	0.14
M-I (B)	0.37	0.591	0.386	0.143	0.062	0.65	0.24	0.10
M-SS (T)	0.30	0.435	0.254	0.158	0.023	0.58	0.36	0.05
M-SS (B)	0.32	0.470	0.261	0.150	0.059	0.56	0.32	0.13
M-AS (T)	0.29	0.399	0.236	0.150	0.013	0.59	0.38	0.03
M-AS (B)	0.29	0.406	0.238	0.157	0.011	0.59	0.39	0.03

*: measured in MIP-experiments

759

760 Table 6: SSA-values of different samples obtained by means of BET and *t*-plot

Sample	Samp. part	Height	BET			t-plot	
		h	V_m[a]	C[b]	S_{Tot}[c]	$V_{\mu pores}$[d]	S_{Tot}[c]
		[mm]	[cm³/g]	[-]	[m²/g]	[cm³/g]	[m²/g]
C-I	Bottom	3	8.39	274	37	0.0029	37
	Middle	15	8.39	274	37	0.0029	37
	Top	27	8.39	274	37	0.0029	37
M-I	Bottom	3	7.43	431	32	0.0043	31
	Middle	15	7.43	431	32	0.0043	31
	Top	27	7.43	431	32	0.0043	31
M-SS	Bottom	3	7.44	331	33	0.0032	32
	Middle	15	7.37	875	32	0.0032	32
	Top	27	7.00	964	31	0.0052	29
M-AS	Bottom	3	7.36	435	32	0.0039	31
	Middle	15	7.23	697	32	0.0039	31
	Top	27	7.00	762	31	0.0046	29

[a]: Associated monolayer capacity; [b]: BET energy constant; [c]: Total specific surface area; [d]: Equivalent specific volume of micropores

761

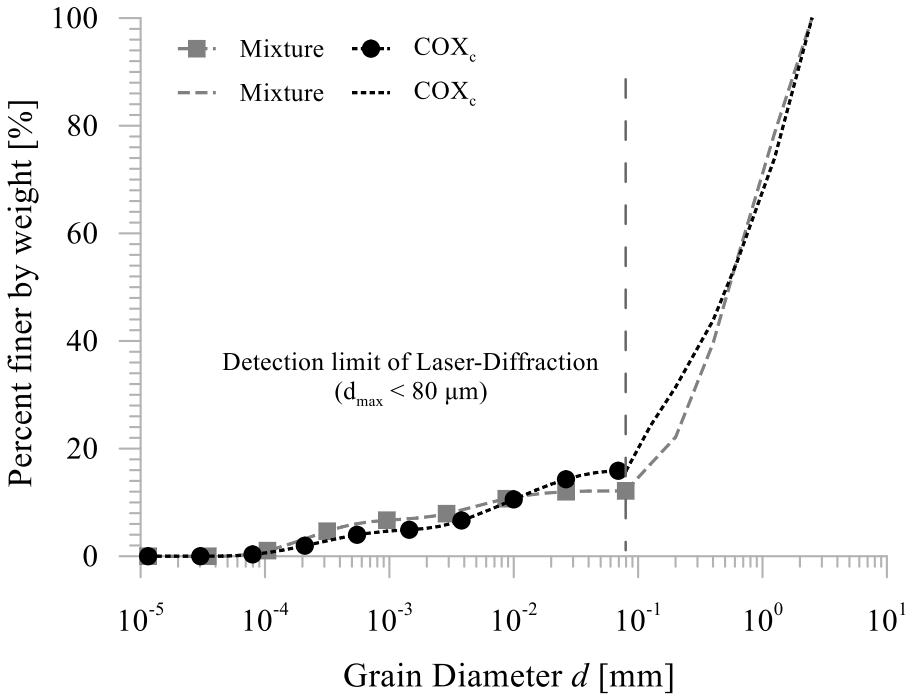

Figure 1: Grain size distribution curves of COX_c and the mixture obtained by dry sieving and laser diffractometry (Middelhoff et al., 2020)

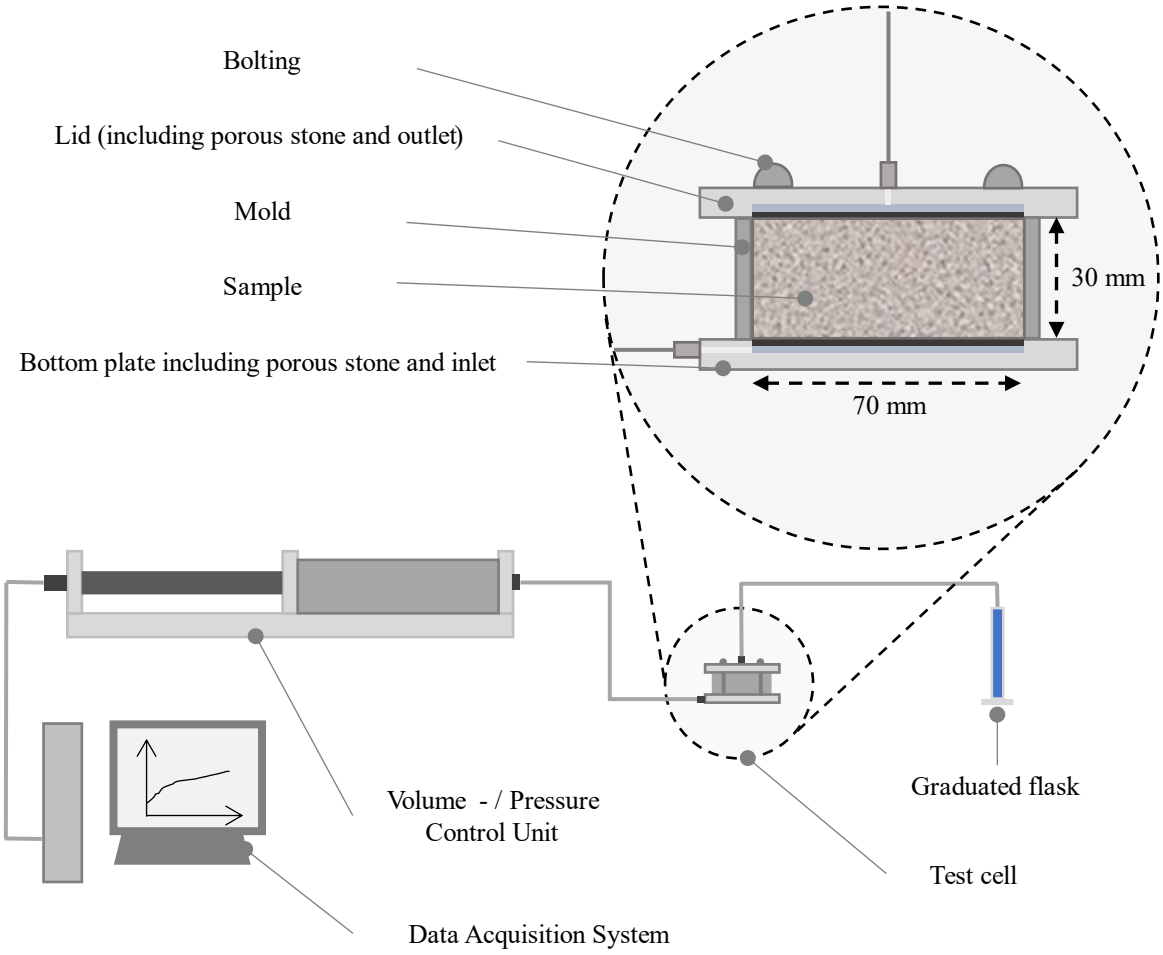

767

768 Figure 2: Setup of hydraulic conductivity experiments

769

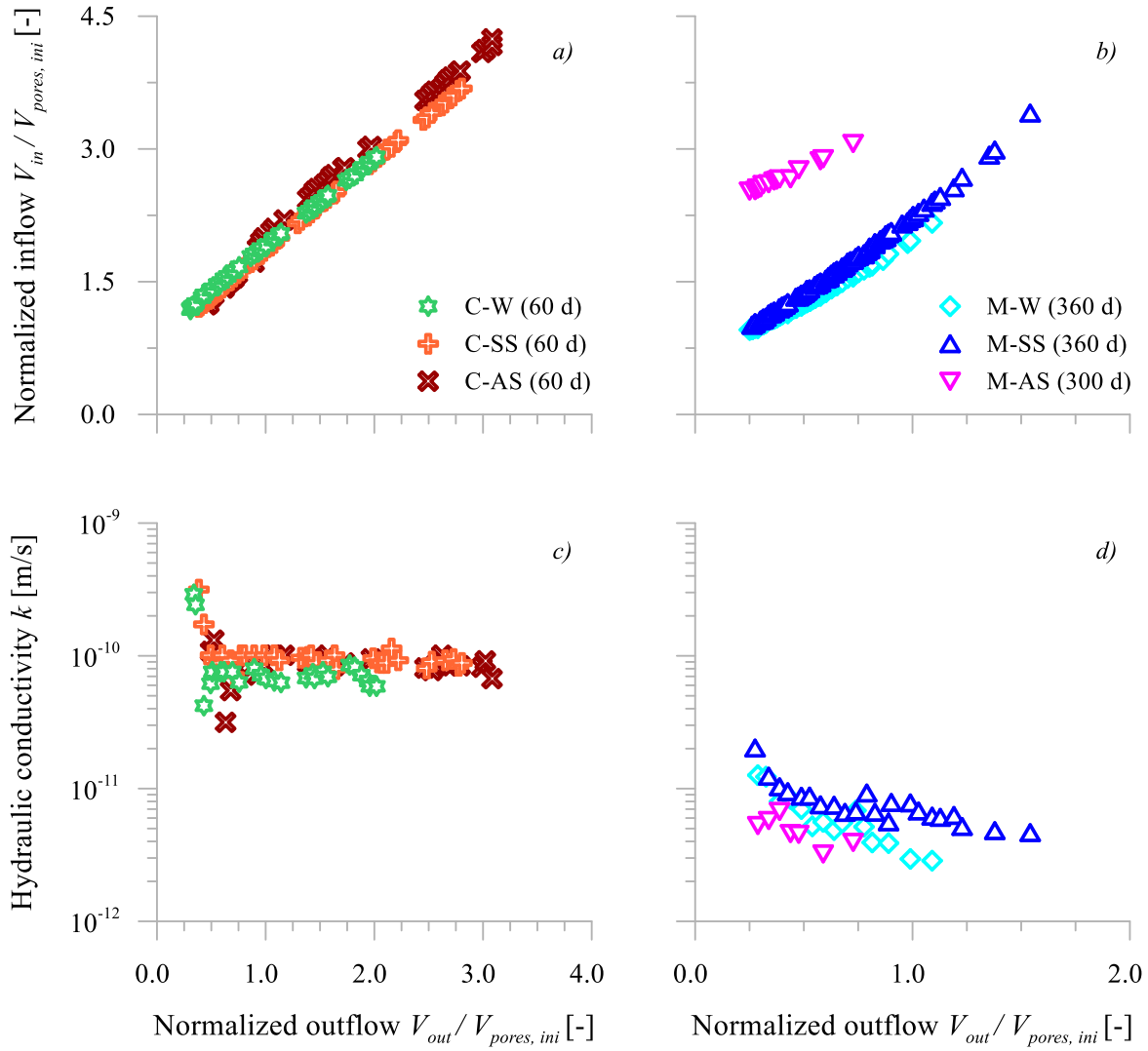

Figure 3: Evolution of the normalized inflow and the hydraulic conductivity of a, c) COX_c ($\rho_{d, ini}$ = 1.95 Mg/m³) and b, d) the mixture ($\rho_{d, ini}$ = 1.72 Mg/m³) as function of the normalized outflow (saturated with water (-W), site solution (-SS) and alkaline solution (-AS))

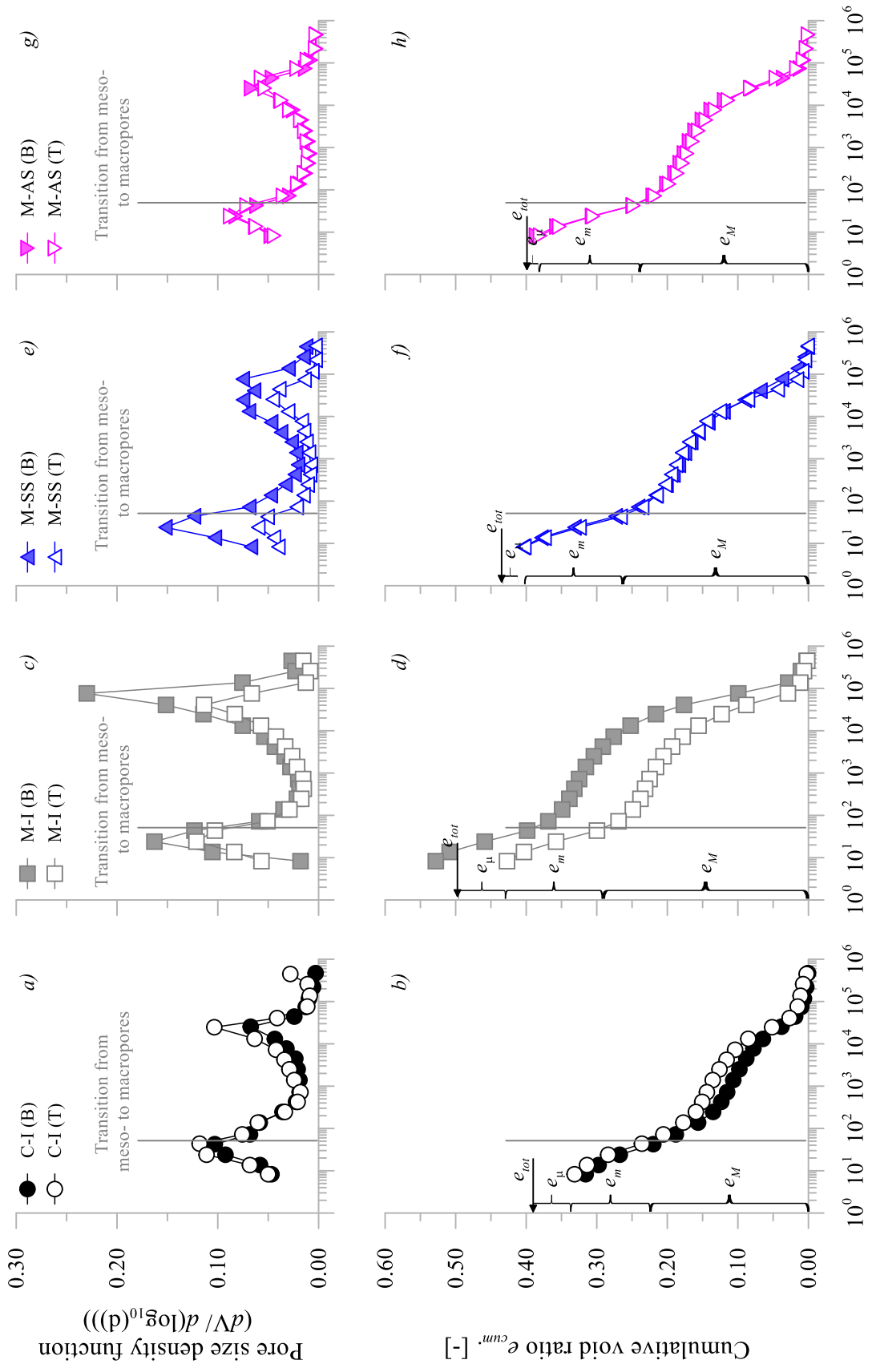

775

776 Figure 4: Results of mercury intrusion porosimetry (MIP) experiments conducted on the top and bottom parts of
777 samples C-I, M-I, M-SS and M-AS

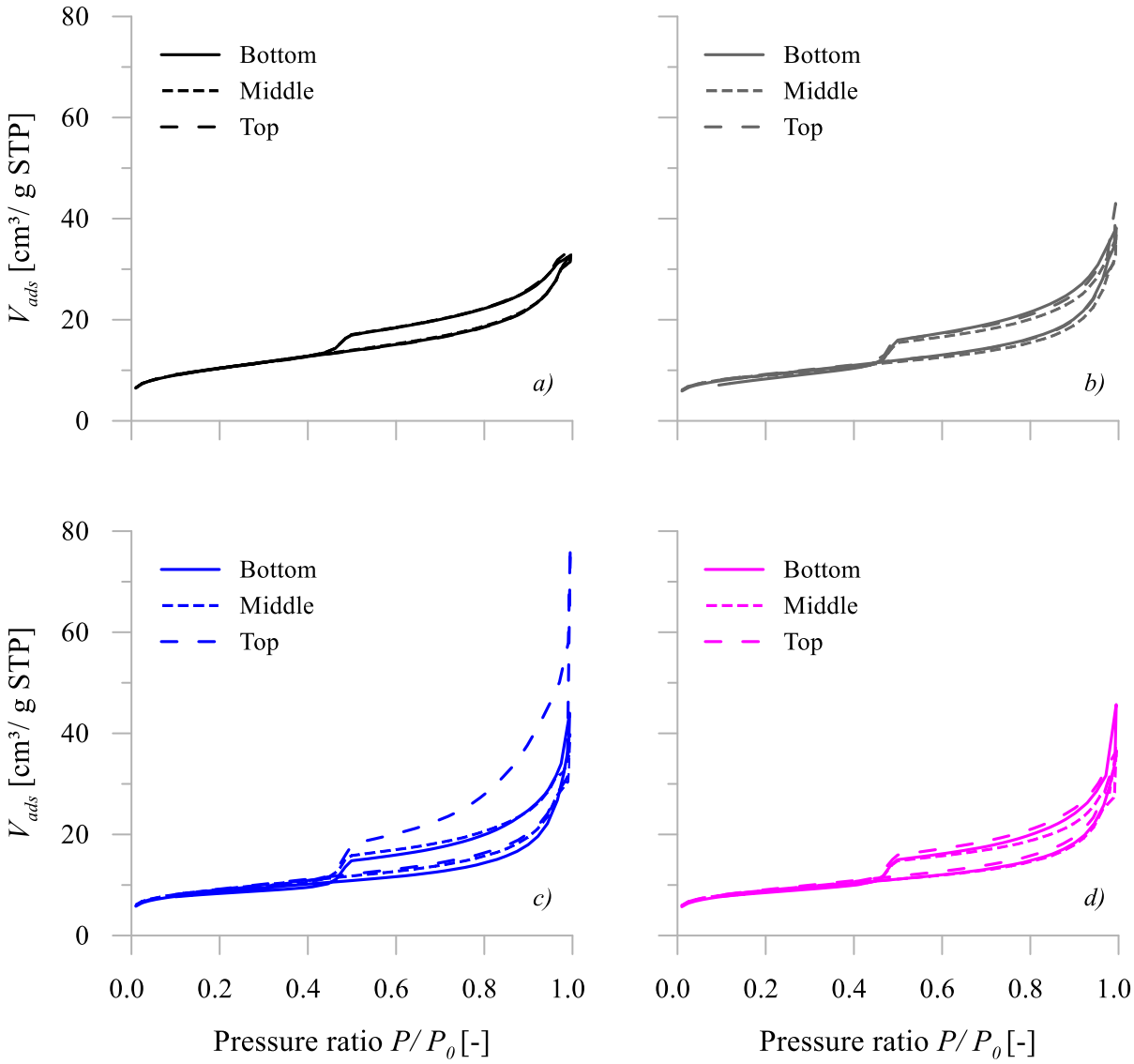

Figure 5: Isotherms* obtained by means of N_2-sorption experiments conducted on the top (27 mm), middle (15 mm) and bottom parts (3 mm) of samples C-I, M-I, M-SS and M-AS (* Pressure ratio versus volume of gas adsorbed (V_{ads}) at standard pressure and temperature (SPT))